Available online at www.sciencedirect.com

ScienceDirect

Ceramics International 40 (2014) 7775–7782

CERAMICS INTERNATIONAL

www.elsevier.com/locate/ceramint

Consolidation of nanoparticle suspensions by centrifugation in non-porous moulds

Martin Trunec[a,b,*], Jiri Misak[b,1]

[a]CEITEC - Central European Institute of Technology, Brno University of Technology, 616 00 Brno, Czech Republic
[b]Institute of Materials Science and Engineering, Brno University of Technology, 616 69 Brno, Czech Republic

Received 2 December 2013; received in revised form 25 December 2013; accepted 26 December 2013
Available online 3 January 2014

Abstract

Alumina and zirconia nanosuspensions with a mean particle size of 100 nm and 15 nm, respectively, were consolidated by centrifugal compaction in non-porous moulds. The nanosuspensions consolidated by high-speed centrifugation were deposited irregularly, resulting in a powder deposit with density profile. The homogeneity of the powder deposits was described and homogeneous and well packed deposit regions were identified. Plate-like bodies were prepared from the homogeneous regions of the deposit. The advantage of regular and dense nanoparticle packing by centrifugal compaction was demonstrated by fabricating transparent alumina and tetragonal zirconia ceramics. The transparent alumina had an in-line transmission of 55% in the visible light at a thickness of 0.8 mm. The transparent tetragonal zirconia reached a dense microstructure with an average grain size of 65 nm and an in-line transmission of 25% at a thickness of 0.5 mm.

Keywords: A. Suspensions; D. Al_2O_3; D. ZrO_2; Centrifugal compaction

1. Introduction

The utilisation of ceramic nanoparticles represents one of the most challenging tasks in the field of bulk ceramics processing. Due to an inherent tendency of nanoparticles to strong agglomeration, the compacted green bodies show an irregular and loosely packed structure. Colloidal processing of nanoparticles is a useful approach to dispersing and/or removing the agglomerates and obtaining stable and well-dispersed nanoparticle suspensions [1]. To fully exploit the advantages of colloidal processing, ceramic bodies must be formed directly from the slurry state [2]. However, the consolidation of ceramic nanosuspensions brings extraordinary difficulties. Direct-casting methods such as direct coagulation casting or gelcasting require high powder loading, which can be difficult to reach in nanoparticle suspensions [3]. Slip casting of nanosuspensions is limited by the low suction power of common porous moulds. Moreover, this suction decreases with increasing sediment thickness [4]. Similar problems with filter and sediment permeability can also be found in pressure filtration [5]. Alternative approaches to the processing of low-concentration nanoparticle suspensions must therefore be used. This contribution investigates a simple alternative method for consolidating nanoparticle suspensions into a bulk ceramic body, using centrifugal forces. During centrifugal consolidation in non-porous moulds the centrifugal force is acting on every ceramic particle in the suspension. The particles move in the direction of the acceleration and deposit on the mould wall, whereas the solvent moves in the opposite direction. The solvent is neither transported through the deposit (as in slip casting or pressure filtration) nor stays in the particle compact formed (as in direct coagulation casting or gelcasting). The drawback of the centrifugal consolidation method is the possible particle size segregation and microstructural gradient development in the deposit due to different settling of particles of different sizes and/or densities. This can be eliminated by

*Corresponding author at: CEITEC - Central European Institute of Technology, Brno University of Technology, 616 00 Brno, Czech Republic. Tel.: +420 541143339; fax: +420 541143202.
E-mail address: trunec@fme.vutbr.cz (M. Trunec).
[1]Present address: sia Abrasives Industries AG, Frauenfeld CH-8501, Switzerland.

0272-8842/$ - see front matter © 2014 Elsevier Ltd and Techna Group S.r.l. All rights reserved.
http://dx.doi.org/10.1016/j.ceramint.2013.12.120

using weakly flocculated suspensions (prepared from dispersed suspensions by adding a large amount of indifferent electrolyte) that are characterised by high viscosity with a pronounced yield stress [6]. Such an approach, however, results in a low-density deposit often with an inhomogeneous density profile [7–9]. A more suitable approach to overcoming the particle size separation problem utilises highly concentrated dispersed suspensions. The mass segregation can be avoided by hindered sedimentation in these high-solid-content suspensions [10,11]. It has been reported that even phase segregation in a composite system Al_2O_3/ZrO_2 could be successfully avoided using a concentrated suspension [12]. Moreover, a well-dispersed suspension produces a dense and regularly packed particle deposit that exhibits good sintering behaviour and a defect-free microstructure [10,13–15].

The sedimentation of dispersed colloidal suspensions with spherical and monosized particles in submicron range meets the condition for creeping flow that can be described by the equation [16]

$$\frac{dr}{dt} = K(\phi)\frac{d^2(\rho_s - \rho_l)g_0}{18\eta} \quad (1)$$

where dr/dt denotes the sedimentation rate, d is the particle diameter, ρ_s and ρ_l are the density of the particles and the liquid, respectively, η denotes the liquid viscosity, and g_0 is the particle acceleration. For centrifugal deposition $g_0 = r\omega^2$, where r is the centrifugal radius and ω is the angular speed. This equation describes the Stokes law for an isolated sphere modified by $K(\phi)$ so as to allow formally for an increase in fluid drag due to hydrodynamic interactions in the multiparticle system. This model assumes no other interaction between particles, except hydrodynamic effects. Brady and Durlofsky [17] have suggested a simple analytical expression for $K(\phi)$:

$$K(\phi) = 1 + \phi - 0.2\phi^2 - \frac{6\phi}{5}\left(\frac{5 - \phi + 0.5\phi^2}{1 + 2\phi}\right) \quad (2)$$

where ϕ denotes the particle volume fraction. Another correction was derived by Barnea and Mizrahi [18]:

$$K(\phi) = \frac{1 - \phi}{(1 + \phi^{1/3})\exp\{5\phi/3(1 - \phi)\}} \quad (3)$$

Dilute suspensions ($\phi < 0.1$) are sufficiently well described by Eqs. (2) and (3) but the behaviour of suspensions deviates from these models at a higher volume loading. Therefore Richardson and Zaki [19] have proposed an empirical correlation in the general form

$$K(\phi) = (1 - \phi)^{\alpha} \quad (4)$$

with $\alpha \approx 5$. Buscall et al. [20] have shown that the value $\alpha = 5.4$ gives a good fit for the suspension of silica particles with a diameter of 200 nm in a range of solid volume fraction from 0 to 0.5.

Centrifugal consolidation of nanosuspensions brings additional difficulties compared with submicron suspensions. It is not only the smaller particle size that makes the dispersed nanoparticles more stable against deposition. The surface forces become increasingly important and change the behaviour of dispersed nanoparticles. The adsorbed ions or polymer species increase the effective volume of dispersed nanoparticles and decrease their overall density [21]. Also the interparticle interactions play a more important role in nanosuspensions than in submicron suspensions because of the much closer contact between nanoparticles at the same suspension loading. Due to these reasons the commonly used centrifugal accelerations in the range of 10^3–$10^4 g$ (where g is the gravitational acceleration) are not sufficient to deposit the nanoparticles and the acceleration has to be increased above $10^4 g$ [22].

Although many investigations have proved the efficiency of centrifugal consolidation for the submicrometre-sized particle suspensions [10,12–15,23], reports on centrifugation of ceramic nanosuspensions are limited. Therefore the objective of the present work was an investigation of centrifugal consolidation of ceramic nanosuspensions and the evaluation of the resulting nanoparticle deposit from the viewpoint of obtaining dense, defect-free nanostructural ceramics.

2. Experimental procedure

Alumina powder (Taimicron TM-DAR, Taimei Chemicals Co., Japan) with a mean particle size of about 100 nm and a specific surface area of 14.5 $m^2\,g^{-1}$ was used for the preparation of alumina suspensions (see Fig. 1). A commercial dispersant, Dolapix CE 64 (Zschimmer & Schwarz, Germany), was used (1 wt% of ceramic powder) to stabilise alumina particles in the water suspension. Suspensions with two volume loadings were prepared, namely with 20 and 47.5 vol % ceramic powder. The ceramic suspensions were treated with ultrasound for 10 min and mixed for 24 h prior to centrifugation. The suspensions were poured into a two-part mould-container with rubber insert (Fig. 2) and then centrifuged (3K30, Sigma, Germany) with centrifugal accelerations of 12,500g, 25,200g, and 54,500g for 5, 10, and 20 min. The schematic diagram of the centrifuge with the mould is shown in Fig. 3. The mould design enabled removing the deposit from

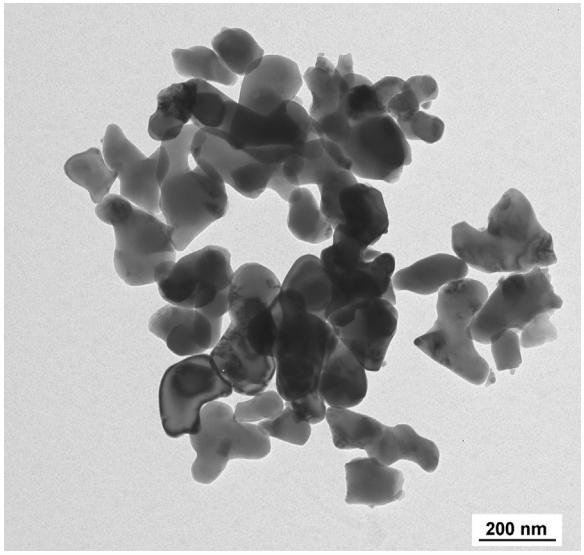

Fig. 1. TEM micrograph of alumina powder.

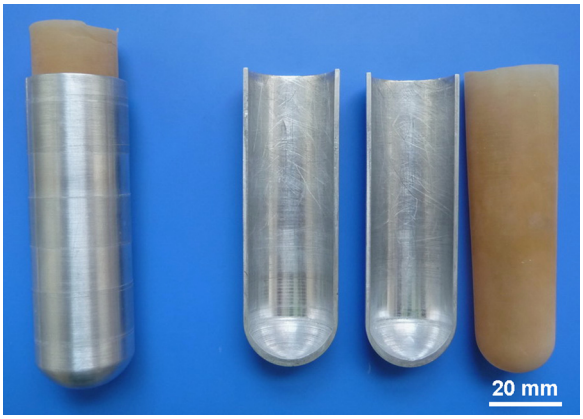

Fig. 2. Two-part mould with a rubber insert.

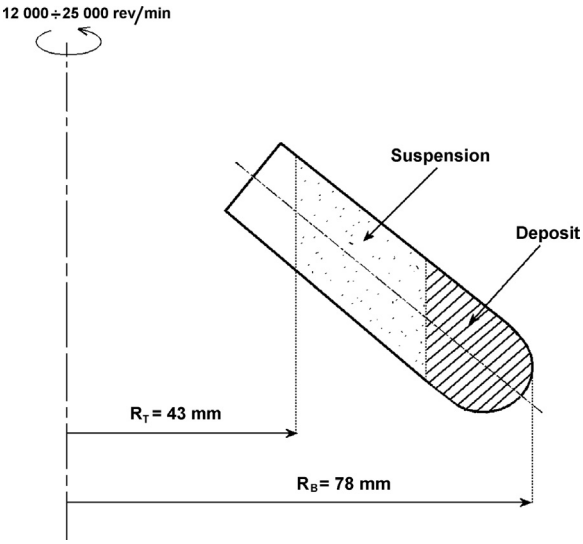

Fig. 3. Schematic diagram of a centrifuge with the mould.

the mould immediately after the centrifugation without any drying. The centrifuged deposit was dried outside the mould at ambient temperature for 3 days, presintered at 800 °C, and finally sintered at 1300 °C for 2 h. For the sake of comparison the same powder was isostatically pressed at 300 MPa to produce a disc-like body with a diameter of 30 mm and a thickness of 10 mm.

Additionally, zirconia nanopowder stabilized by 3 mol% yttria (MELox Nanosize 3Y, Mel, UK), supplied as a stable 5 vol% water suspension, was used for the centrifugal compaction experiments. The dispersed particles with a size of 10–15 nm (see Fig. 4) were stabilized in the acidic region. To obtain a reasonably large deposit the zirconia suspension had to be osmotically concentrated in a 40% water solution of polyethylene oxide (M_w=35,000) using a tube membrane (SpectraPor 3, Spectrum Laboratories, USA). The concentrated zirconia nanosuspension contained 14 vol% of solids prior to centrifugation. The highest centrifugal acceleration of 54500g was applied for 10 and 30 min to deposit the zirconia nanoparticles. The centrifuged deposit was dried at ambient temperature and controlled humidity for several days,

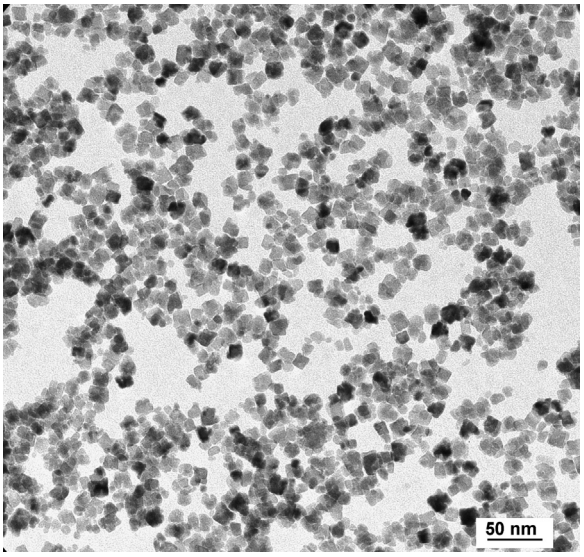

Fig. 4. TEM micrograph of tetragonal zirconia powder.

optionally presintered at 600 °C, and finally sintered at 1100 °C for 1.5 h.

The pore size distribution in green and partially sintered bodies was investigated via mercury intrusion porosimetry (Pascal 440, Porotec, Germany). The densification curves were determined using a high-temperature dilatometer (L75/50, Linseis, Germany). The density of green and sintered bodies was determined by the Archimedes method. The relative densities of ceramic bodies were calculated using the values 3.987 and 6.08 g cm^{-3} for the theoretical density of alumina and tetragonal zirconia, respectively. The green densities were measured at least three times for each sample and the difference from the mean was less than $\pm$0.2% t.d. for green bodies and $\pm$0.03% t.d. for sintered bodies. The average grain size of sintered bodies was determined using the linear intercept method on at least three SEM micrographs of polished and thermally etched samples. The linear intercept grain size was corrected by a factor of 1.56 to yield the true grain size [24].

The transparent bodies were prepared by pressureless presintering in air followed by hot isostatic pressing in a graphite-free press (ABRA Shirp, Switzerland) at 198 MPa of argon. Real in-line transmission (RIT) of polished samples was measured with a He–Ne laser (λ=632.8 nm), the distance from the sample to the detector was 860 mm (with an opening angle of 0.5°).

3. Results and discussion

3.1. Alumina suspensions

The characteristic shape of a powder deposit after centrifugation is shown in Fig. 5a. The irregular shape of the deposit resulted from the use of a fixed-angle rotor for high centrifugal forces. Using this rotor the powder was not deposited exactly

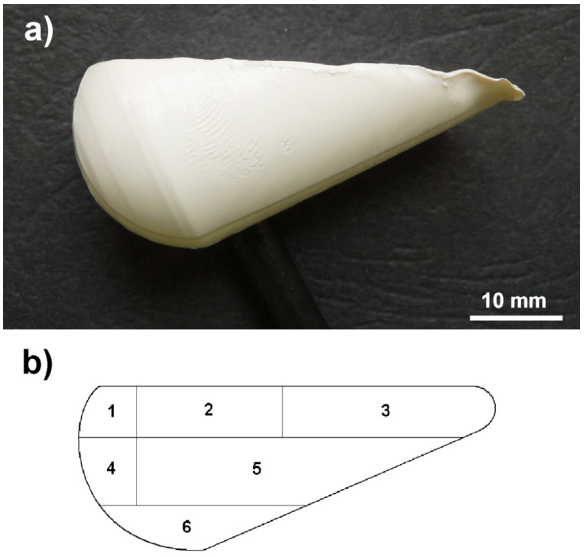

Fig. 5. (a) Photograph of a powder deposit after centrifugation and (b) partitioning of the powder deposit.

in the vertical direction of the mould. The powder deposit was stiff enough to be removed from the rubber mould and handled. The packing density of the deposit was higher than that of the isostatically pressed body (~62% vs. 56.3%). However, the difference between the centrifuged and the pressed powders diminished after sintering and no clear dependence of sintering density on centrifugal acceleration and time could be inferred. Moreover, the centrifuged bodies exhibited substantial density inhomogeneity. This inhomogeneity manifested itself by cracks and different translucency of the sintered body.

The presintered centrifuged bodies were, therefore, divided into several pieces (see Fig. 5b), which were sintered and evaluated separately. The evaluation of the individual parts confirmed the inhomogeneity of the presintered as well as the sintered centrifuged bodies. Tables 1 and 2 show the relative densities of individual presintered and sintered parts centrifuged from both the 47.5 and the 20 vol% suspensions at a centrifugal acceleration of 54500g and 12500g for 10 min. A centrifugation time of 10 min was taken as a standard because there were no detectable differences between 5, 10 and 20 min of centrifugation. Low packing and sintering densities were identified in region 6 (see Fig. 5b), i.e. in the deposition region where the powder was deposited first. On the other hand, the packing and sintering densities were high and homogeneous in regions 1, 2, 3, and 5. An evaluation revealed that the highest sintered densities in deposit regions 1–3 and 5 were obtained with the high-concentrated suspension (47.5 vol %) centrifuged at the highest centrifugal speed. The sintered densities obtained from the low-concentrated suspension (20 vol%) were only slightly lower but the whole deposit was much more homogeneous than in the previous case. In both cases the sintered relative densities of the "high-density" regions (1–3, 5) were higher than the density of the CIPed body (99.6–99.9% vs. 99.2%).

Table 1
Relative densities of individual presintered and sintered parts of the deposits centrifuged from the 47.5 and 20 vol% alumina suspensions at a centrifugal acceleration of 54500g for 10 min.

Section	47.5 vol%		20 vol%	
	800 °C/0 h	1300 °C/2 h	800 °C/0 h	1300 °C/2 h
1	63.0	99.75	60.9	99.56
2	63.3	99.85	61.7	99.61
3	64.2	99.85	61.2	99.49
4	62.7	99.03	61.2	99.22
5	62.8	99.53	62.3	99.40
6	60.1	98.21	61.6	98.38

Table 2
Relative densities of individual presintered and sintered parts of the deposits centrifuged from the 47.5 and 20 vol% alumina suspensions at a centrifugal acceleration of 12500g for 10 min.

Section	47.5 vol%		20 vol%	
	800 °C/0 h	1300 °C/2 h	800 °C/0 h	1300 °C/2 h
1	63.5	99.70	62.7	99.51
2	63.4	99.69	62.7	99.61
3	63.9	99.79	62.9	99.68
4	62.8	98.98	62.8	99.41
5	63.2	99.64	63.1	99.60
6	59.4	97.47	62.6	98.92

To explain the deposition behaviour of alumina suspensions we need to compare our centrifugal experiments with the creeping model discussed in the Introduction. After integrating Eq. (1) and combining with (4) we obtain the following expression for the total deposition time:

$$t = \frac{18\eta}{(1-\phi)^{5.4} d^2 (\rho_s - \rho_l)\omega^2} \ln\left(\frac{r_B}{r_T}\right) \quad (5)$$

where r_B and r_T are the radial positions of the bottom and the top of the mould, respectively. The graph in Fig. 6 shows the model deposition time of the particles moving from the top of the mould to the bottom during centrifugation. The time for increasing the rotation speed to the nominal value at the start of centrifugation was ignored in the calculation because the sedimentation is negligible in this time period. It follows from the graph in Fig. 6 that the calculated time for the full deposition exceeds the real deposition time (< 300 s) substantially, especially for highly concentrated suspensions. Thus it results from this comparison that the investigated suspensions do not follow the Stokes law during centrifugation. The deviation from the theory was most probably caused by interactions between nanoparticles, and these interactions were more pronounced in concentrated suspensions. In such suspensions the nanoparticles might behave as clusters of weakly flocculated particles during centrifugation. However, no exact description of the sedimentation of such systems is currently available. We can conclude that even in well-dispersed highly-concentrated

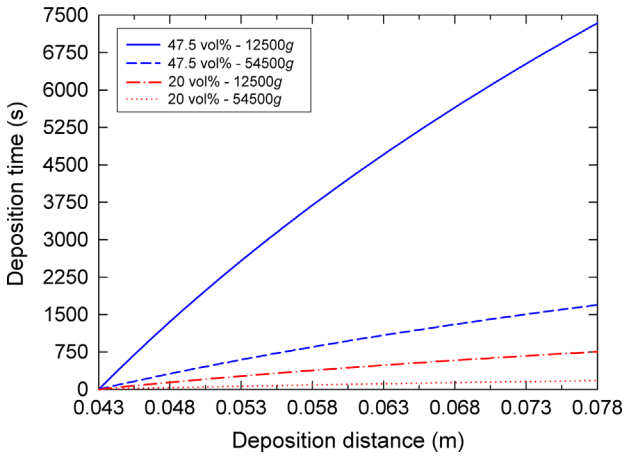

Fig. 6. Deposition time of alumina particles as a function of deposition distance.

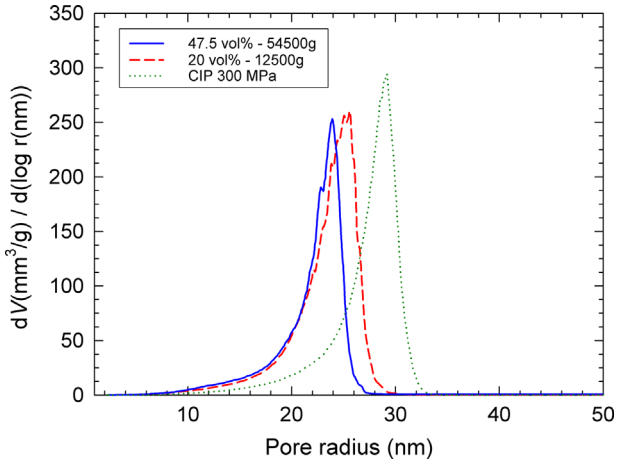

Fig. 7. Pore size distribution of presintered (800 °C) alumina deposits.

nanosuspensions the restricted movement of depositing nanoparticles at the beginning of high-speed centrifugation did not allow regular packing of the deposit. The arrangement of particles was restricted by interaction with their neighbours and only later during the deposition, when the suspension concentration decreased, was there enough space for the remaining individual particles to rearrange into a more regular deposit. This hypothesis can also explain the more homogeneous deposit obtained with the low-concentrated suspension. Thus there is a clear difference in the deposit homogeneity between the high-speed centrifugation of nanosuspensions and the low-speed centrifugation of sub-micron suspensions. The latter was reported [10] to have produced even complex deposits from concentrated suspensions with homogeneous structure.

To obtain homogeneous ceramic bodies from our deposits, plates ($30 \times 20 \times 4$ mm^3) were cut from the homogeneous regions (1–3, 5) of the deposits immediately after centrifugation and prior to drying. These ceramic plates were carefully investigated. The graph in Fig. 7 shows the pore size distribution in presintered plates (800 °C). The centrifuged bodies are compared with the isostatically pressed body. The graph shows a preferential particle packing in the centrifuged

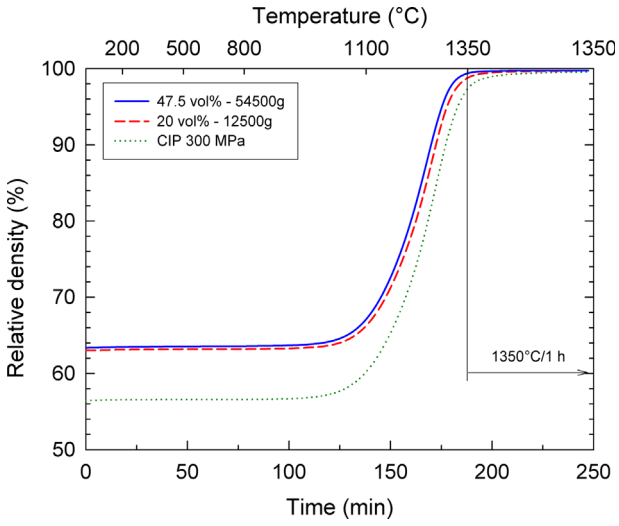

Fig. 8. Sintering curves of centrifuged and CIP alumina bodies.

bodies. The high-concentrated suspension provided only a slightly better packing than the low-concentrated suspension. The graph in Fig. 8 compares the sintering curves of centrifuged and pressed bodies. It is not surprising that the better packing of centrifuged bodies resulted in an easier densification compared with the pressed body. Even the slightly better packing of the body formed from high-concentrated suspension could be detected on the sintering curves. Both centrifuged alumina ceramics reached 99.7% of theoretical density after sintering at 1350 °C for 1 h.

3.2. Zirconia suspension

The mean particle size of alumina powder (~100 nm) lies on the upper edge of the nanometre range. The method of centrifugal consolidation developed with this powder was also applied to a fine zirconia nanosuspension with a particle size in the range of 10–15 nm. The zirconia nanosuspension was consolidated at the highest centrifugal acceleration (54500g) for 10 and 30 min. After 10 min of centrifugation the zirconia particles were not fully deposited at the bottom of the mould, whereas after 30 min only a pure supernatant was found above a dense deposit. The centrifugation time correlated quite well with the model that predicted a total deposition time of 20 min. It seems that low-concentrated suspensions better comply with the conditions of creeping flow. Nevertheless, even this deposit was not fully homogenous. Because of the lower solid loading in the zirconia suspension (14 vol%) the zirconia deposit was smaller than that of alumina but it was possible to cut a homogeneous plate ($15 \times 10 \times 2$ mm^3) from the wet deposit. The densely packed regions in the deposit were easily distinguished by their translucency. Fig. 9 shows a dried zirconia plate with a relative density of 46%. The partial transparency of the dried zirconia deposit is a confirmation of the regular packing of nanoparticles with homogeneous distribution of very small pores [25]. The pore size analysis in the dried deposit (see Fig. 10) confirmed that the pores were extremely small and with a narrow size distribution (2–4 nm).

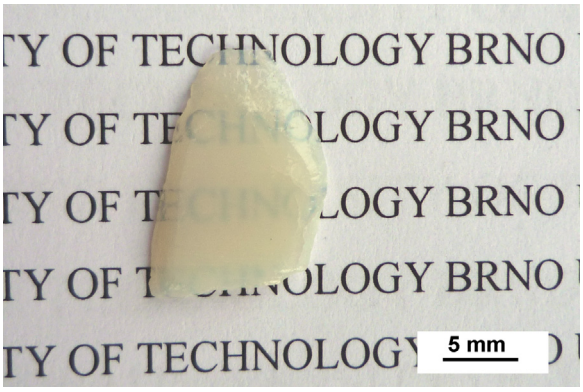

Fig. 9. Dried zirconia deposit with a relative density of 46%.

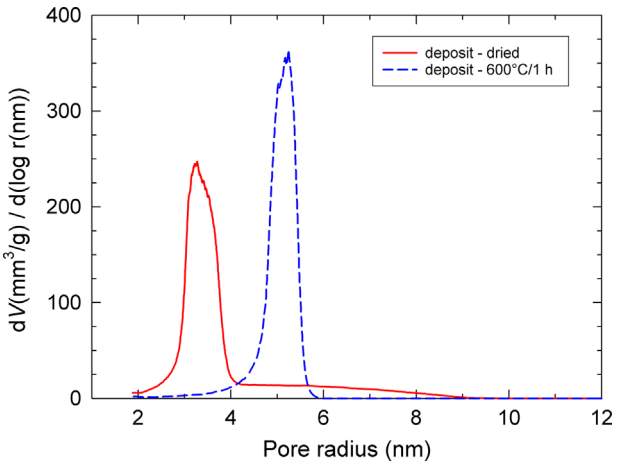

Fig. 10. Pore size distribution of dried and preheated zirconia deposits.

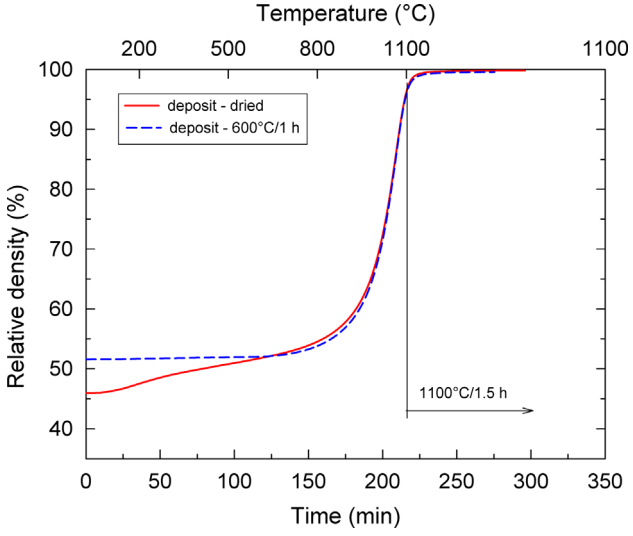

Fig. 11. Sintering curves of centrifuged zirconia bodies.

The tail of the distribution at higher pore sizes is not caused by the presence of larger pores but is a result of a compression of adsorbed moisture and other species on the nanoparticle surface. After heating to 600 °C these adsorbents were removed and the compressibility disappeared. The particle rearrangement during the removal of adsorbed layers increased slightly the pore size. This hypothesis was confirmed by the dilatometric curves of these bodies during sintering (see Fig. 11). The preheated body lacked the moderate shrinkage at low temperatures (up to 600 °C) but the rest of the curves was identical. Because no sintering can be expected at temperatures of 200–300 °C, the shrinkage must have been connected with a removal of adsorbed species. A similar effect was also reported in pressed nanoparticle compacts [26,27]. The centrifuged zirconia bodies could be sintered to almost full density (99.8% t.d.) at a temperature of 1100 °C for 1.5 h. The average grain size in sintered body was 136 nm.

3.3. Transparent alumina and tetragonal zirconia ceramics

The ability to obtain regular and defect-free particle packing via centrifugal deposition was demonstrated by the preparation of transparent samples. The above-mentioned alumina plates were densified to almost 100% of theoretical density without defects and pores that would scatter light. The plates prepared from the 47.5 vol% (centrifuged at 54,500 *g*) and 20 vol% (centrifuged at 12,500 g) alumina suspensions were sintered without pressure to the state of closed pores at 1200 °C/2 h and 1220 °C/2 h, respectively, followed by hot isostatic pressing at 1200 °C/3 h and 198 MPa of argon atmosphere. Fig. 12 shows polished transparent plates of ~0.9 mm in thickness. High real in-line transmission (RIT) of alumina sample (RIT = 55% at 633 nm and 0.8 mm thickness) demonstrates the defect-less ceramic structure with small grain size (~600 nm) [28].

The zirconia plate prepared from 14 vol% zirconia suspension was presintered at 1005 °C for 3.5 h and exposed to hot isostatic pressing at 1010 °C/3 h and 198 MPa of argon. The polished zirconia plate is shown in Fig. 13. The real in-line transmission was about 25% (at 633 nm and 0.5 mm thickness), which is comparable to the highest RIT value ever reported for the tetragonal zirconia ceramics [29]. The microphotograph in Fig. 14 presents a nanocrystalline microstructure

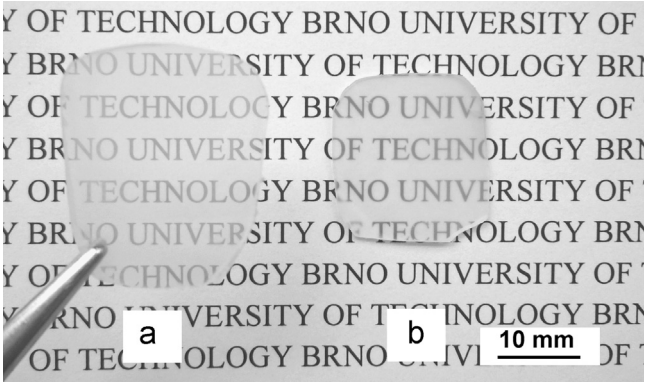

Fig. 12. Transparent alumina plates with a thickness of 0.9 mm (a) 30 mm above the text; (b) on the text.

of the transparent zirconia. The average grain size of this microstructure was 65 nm. According to the model developed by Klimke et al. [30] for the dependence of in-line transmission on grain size, the calculated transmission of a dense

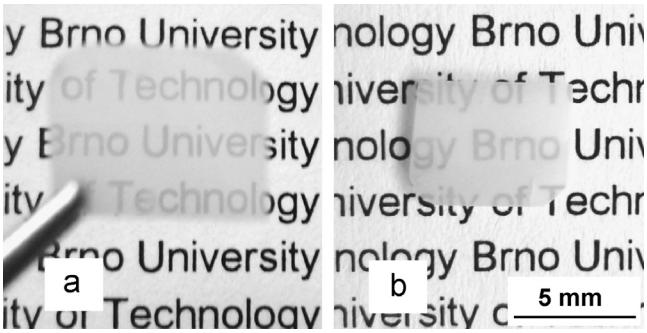

Fig. 13. Transparent tetragonal zirconia plate with a thickness of 0.5 mm (a) 30 mm above the text; (b) on the text.

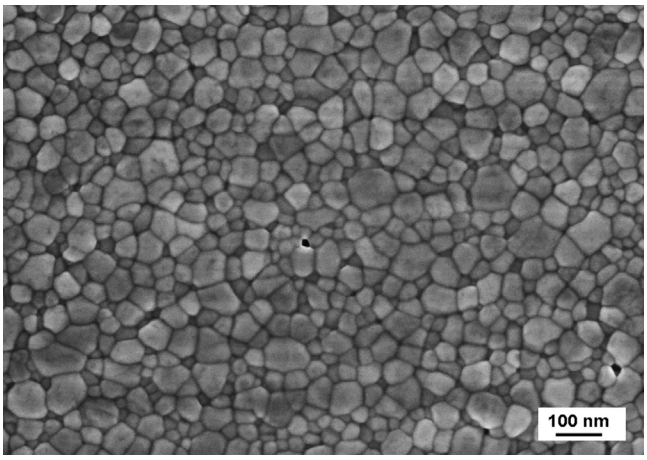

Fig. 14. SEM micrograph of transparent tetragonal zirconia ceramics.

65 nm grain size zirconia corresponds to ~35%. Thus we can conclude that the HIPed zirconia ceramic still contained some residual porosity and we can even expect a transparency improvement after sintering optimisation.

4. Conclusions

Alumina suspensions with a particle size of 100 nm were consolidated in non-porous moulds by centrifugation with a centrifugal acceleration in the range of 12,500–54,500*g*. The homogeneity of centrifuged alumina bodies was described in dependence on the centrifugal force. It was shown that homogenous plate samples with regular particle packing could be obtained from centrifuged bodies. The structure and sintering behaviour of such alumina bodies were superior to samples prepared by cold isostatic pressing. Similar properties were reached in samples prepared from a suspension with high powder loading (47.5 vol%) as well as with lower powder loading (20 vol%). The advantage of regular and dense particle packing by centrifugal compaction was demonstrated by fabricating transparent alumina ceramics with an in-line transmission of 55% (at 633 nm wavelength and 0.8 mm plate thickness). The method of centrifugal compaction was also applied to 14 vol% zirconia nanosuspension with a particle size of 15 nm. A dense deposit could be obtained after centrifugation at the highest centrifugal acceleration of 54500*g* for 30 min. The partial transparency of the dried deposit demonstrated regular packing of zirconia nanoparticles with narrow size distribution of small pores. After hot isostatic pressing the tetragonal zirconia ceramics retained the nanocrystalline structure with an average grain size of 65 nm and an in-line transmission of 25% (at 633 nm wavelength and 0.5 mm plate thickness).

Acknowledgements

The author (M.T.) gratefully acknowledges the funding provided by the Grant Agency of the Czech Republic under Grant no. 13-09310S. This work was realised in CEITEC – Central European Institute of Technology, with research infrastructure supported by the project CZ.1.05/1.1.00/02.0068 financed from European Regional Development Fund.

References

[1] J.A. Lewis, Colloidal processing of ceramics, J. Am. Ceram. Soc. 83 (2000) 2341–2359.
[2] F.F. Lange, Powder processing science and technology for increased reliability, J. Am. Ceram. Soc. 72 (1989) 3–15.
[3] W.M. Sigmund, N.S. Bell, L. Bergstrom, Novel powder-processing methods for advanced ceramics, J. Am. Ceram. Soc. 83 (2000) 1557–1574.
[4] C. Schilling, I.A. Aksay, Slip casting, in: S.J. Schneider (Ed.), Ceramics and Glasses, ASM International, Metals Park, Ohio, 1991, pp. 153–160.
[5] F.F. Lange, K.T. Miller, Pressure filtration – consolidation kinetics and mechanics, Am. Ceram. Soc. Bull. 66 (1987) 1498–1504.
[6] J.C. Chang, B.V. Velamakanni, F.F. Lange, D.S. Pearson, Centrifugal consolidation of Al_2O_3 and Al_2O_3/ZrO_2 composite slurries vs interparticle potentials: particle packing and mass segregation, J. Am. Ceram. Soc. 74 (1991) 2201–2204.
[7] L. Bergstrom, C.H. Schilling, I.A. Aksay, Consolidation behavior of flocculated alumina suspensions, J. Am. Ceram. Soc. 75 (1992) 3305–3314.
[8] J.S. Abel, G.C. Stangle, C.H. Schilling, I.A. Aksay, Sedimentation in flocculating colloidal suspensions, J. Mater. Res. 9 (1994) 451–461.
[9] W.H. Shih, W.Y. Shih, S.I. Kim, I.A. Aksay, Equilibrium-state density profiles of centrifuged cakes, J. Am. Ceram. Soc. 77 (1994) 540–546.
[10] W. Huisman, T. Graule, L.J. Gauckler, Alumina of high-reliability by centrifugal casting, J. Eur. Ceram. Soc. 15 (1995) 811–821.
[11] B.V. Velamakanni, F.F. Lange, Effect of interparticle poentials and sedimentation on particle packing density of bimodal particle distributions during pressure filtration, J. Am. Ceram. Soc. 74 (1991) 166–172.
[12] P.G. Rao, M. Iwasa, T. Tanaka, I. Kondoh, Centrifugal casting of Al_2O_3–15 wt% ZrO_2 ceramic composites, Ceram. Int. 29 (2003) 209–212.
[13] P. Hidber, F. Baader, T. Graule, L.J. Gauckler, Sintering of wet-milled centrifugal cast alumina, J. Eur. Ceram. Soc. 13 (1994) 211–219.
[14] W. Huisman, T. Graule, L.J. Gauckler, Centrifugal slip casting of zirconia (TZP), J. Eur. Ceram. Soc. 13 (1994) 33–39.
[15] J. Koike, S. Tashima, S. Wakiya, K. Maruyama, H. Oikawa, Mechanical properties and microstructure of centrifugally compacted alumina and hot-isostatically-pressed alumina, Mater. Sci. Eng. A—Struct. Mater. Prop. Microstruct. Process. 220 (1996) 26–34.
[16] R. Buscall, The sedimentation of concentrated colloidal suspensions, Colloids Surf. 43 (1990) 33–53.
[17] J.F. Brady, L.J. Durlofsky, The sedimentation rate of disordered suspensions, Phys. Fluids 31 (1988) 717–727.
[18] E. Barnea, J. Mizrahi, A generalized approach to the fluid dynamics of particulate systems, Chem. Eng. J. 5 (1973) 171–189.

[19] J.F. Richardson, W.N. Zaki, The sedimentation of a suspension of uniform spheres under conditions of viscous flow, Chem. Eng. Sci. 3 (1954) 65–73.
[20] R. Buscall, J.W. Goodwin, R.H. Ottewill, T.F. Tadros, The settling of particles through newtonian and non-newtonian media, J. Colloid Interface Sci. 85 (1982) 78–86.
[21] M. Trunec, H. Hrazdera, Effect of ceramic nanopowders on rheology of thermoplastic suspensions, Ceram. Int. 31 (2005) 845–849.
[22] P. Figiel, L. Jaworska, Z. Pedzich, P. Wyzga, P. Putyra, P. Klimczyk, Al_2O_3 and ZrO_2 powders formed by centrifugal compaction using the ultra HCP method, Ceram. Int. 39 (2013) 635–640.
[23] K. Sato, Y. Hotta, H. Yilmaz, K. Watari, Fabrication of green and sintered bodies prepared by centrifugal compaction process using wet-jet milled slurries, J. Eur. Ceram. Soc. 29 (2009) 1323–1329.
[24] M.I. Mendelson, Average grain size in polycrystalline ceramics, J. Am. Ceram. Soc. 52 (1969) 443–446.
[25] V.V. Srdic, M. Winterer, H. Hahn, Sintering behavior of nanocrystalline zirconia prepared by chemical vapor synthesis, J. Am. Ceram. Soc. 83 (2000) 729–736.
[26] K. Maca, M. Trunec, P. Dobsak, Bulk zirconia nanoceramics prepared by cold isostatic pressing and pressureless sintering, Rev. Adv. Mater. Sci. 10 (2005) 84–88.
[27] M. Trunec, K. Maca, Compaction and pressureless sintering of zirconia nanoparticles, J. Am. Ceram. Soc. 90 (2007) 2735–2740.
[28] R. Apetz, M.P.B. van Bruggen, Transparent alumina: a light-scattering model, J. Am. Ceram. Soc. 86 (2003) 480–486.
[29] U. Anselmi-Tamburini, J.N. Woolman, Z.A. Munir, Transparent nanometric cubic and tetragonal zirconia obtained by high-pressure pulsed electric current sintering, Adv. Funct. Mater. 17 (2007) 3267–3273.
[30] J. Klimke, M. Trunec, A. Krell, Transparent tetragonal yttria-stabilized zirconia ceramics: influence of scattering caused by birefringence, J. Am. Ceram. Soc. 94 (2011) 1850–1858.